nature ecology & evolution

SUPPLEMENTARY INFORMATION

VOLUME: 1 | ARTICLE NUMBER: 0003

In the format provided by the authors and unedited.

Plant spatial patterns identify alternative ecosystem multifunctionality states in global drylands

Miguel Berdugo[1]*, Sonia Kéfi[2], Santiago Soliveres[3] and Fernando T. Maestre[1]

Supplementary Figures

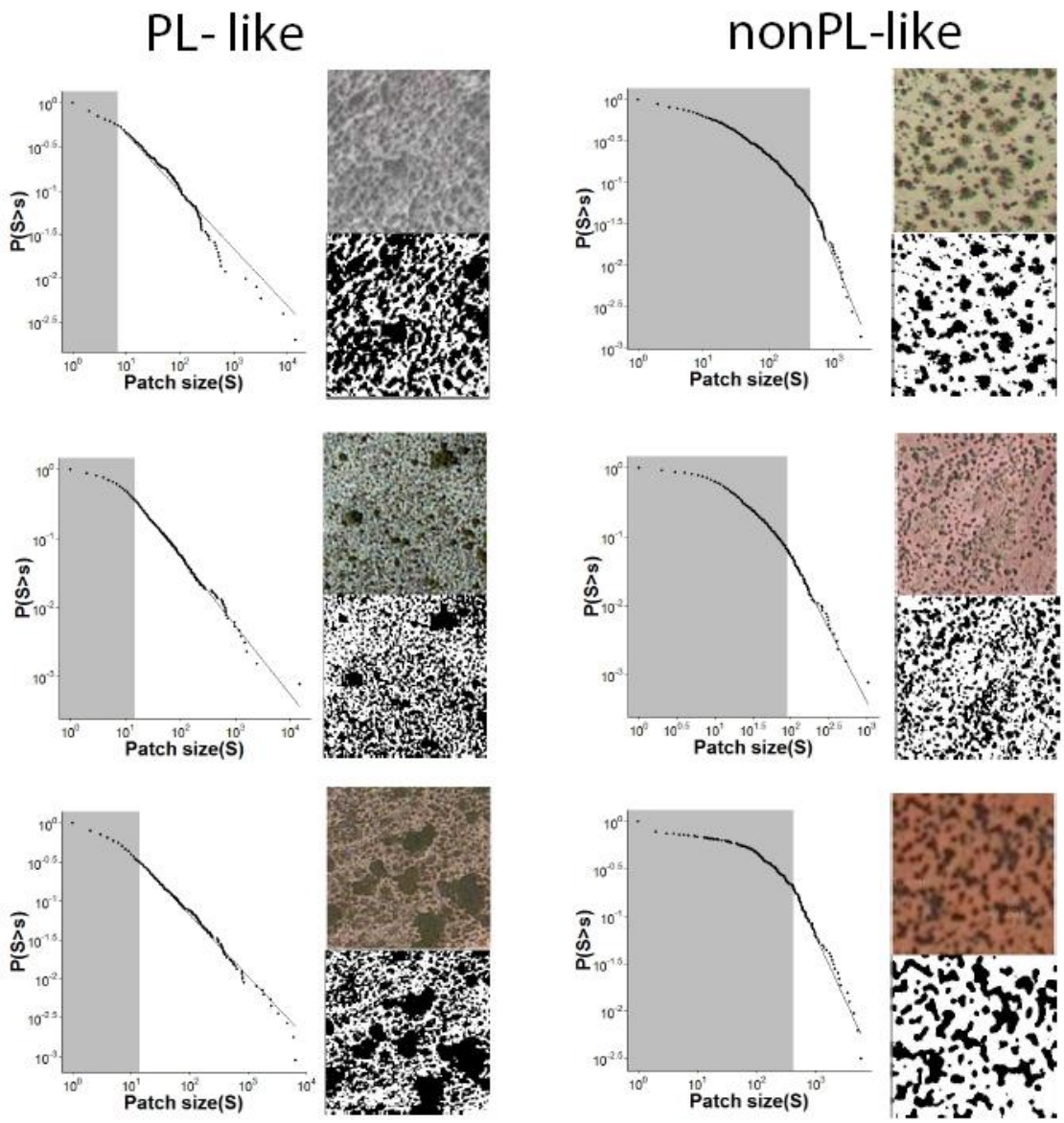

Supplementary Figure 1. Examples of patch-size distributions found in global drylands. Six examples of sites where the patch size distribution of vegetation either follow a power law (PL-like) or not (nonPL-like). The inversed cumulative distributions are shown (both axis are log-scaled). The original image and that resulting from its classification are displayed to the right of each distribution. The shaded area represents data with patch sizes lower than x_{min} (therefore not fitted to power law functions). The

power law range (PLR) corresponds to the percentage of non-shaded area in each distribution. The black line is the fitted power law.

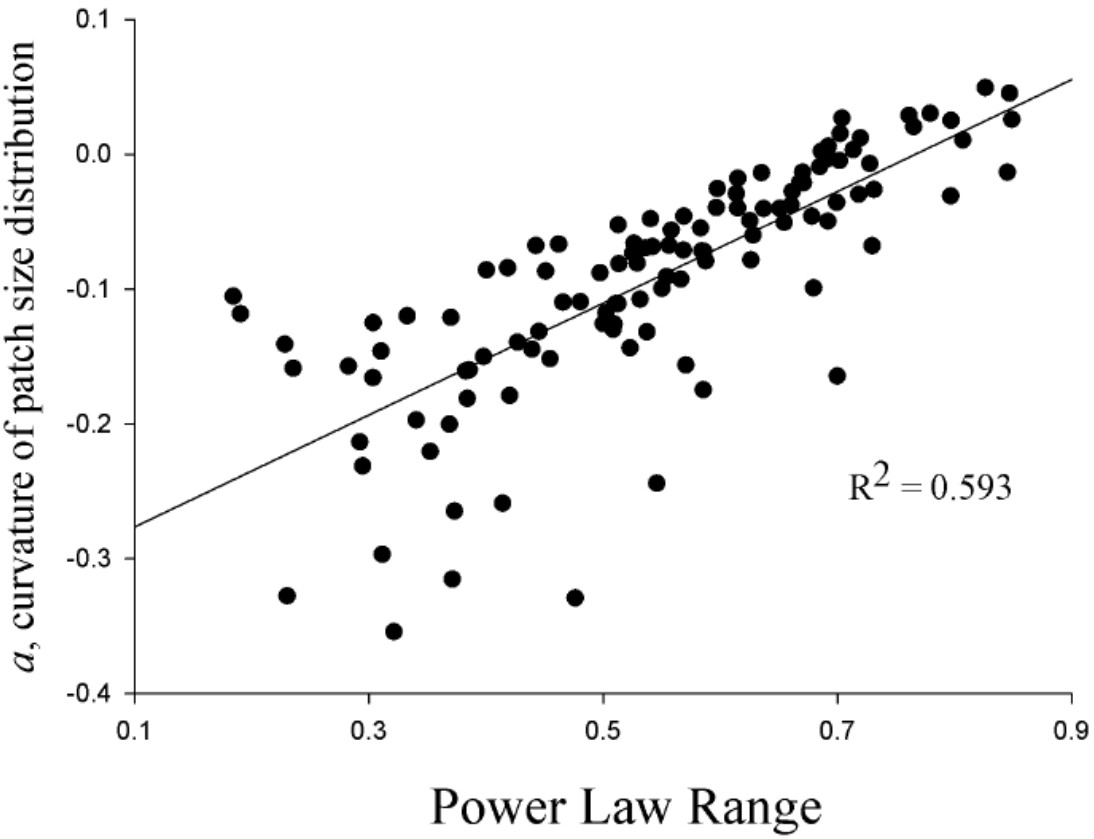

Supplementary Figure 2. Relationship between power law relative range and the shape of patch-size distributions. Relationship between the power law relative range parameter obtained for the patch size distributions and the curvature of the cumulative patch size distribution. The curvature is obtained as the quadratic term (a) from a second degree polynomial regression between patch size and their cumulative frequency (both log-transformed) for every patch size distribution. The parameter *a* indicates concave patch size distributions if negative; convex if positive and straight line if zero. Dashed line indicates $a = 0$. The solid line represents the linear regression between *a* and PLR.

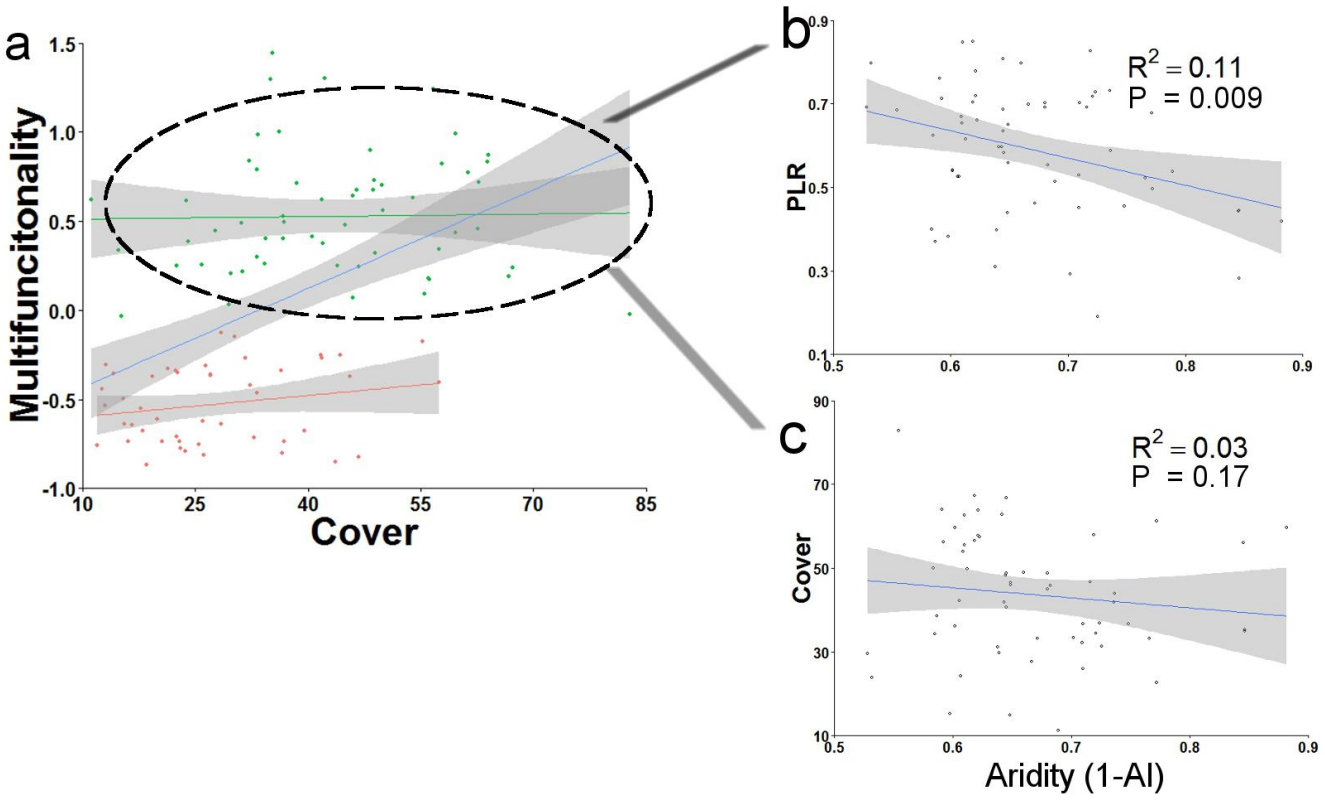

Supplementary Figure 3. Varying relationships between plant cover, patch-size distributions, multifunctionality and aridity. Relationship between total cover and multifunctionality for all our study sites (blue line, F=43.3, P<0.001) and for sites from high (green line, F=0.26, P=0.61) and low (red line, F=4.8, P=0.03) multifunctionality states (a). The right panels show the relationships between aridity (1 – aridity index, AI) and both the power law relative range (PLR, b) and total cover (TCT, c) in the sites from the high multifunctionality state (surrounded by a ellipse in panel a, N = 53). The shaded areas indicate the confidence intervals of the linear regressions.

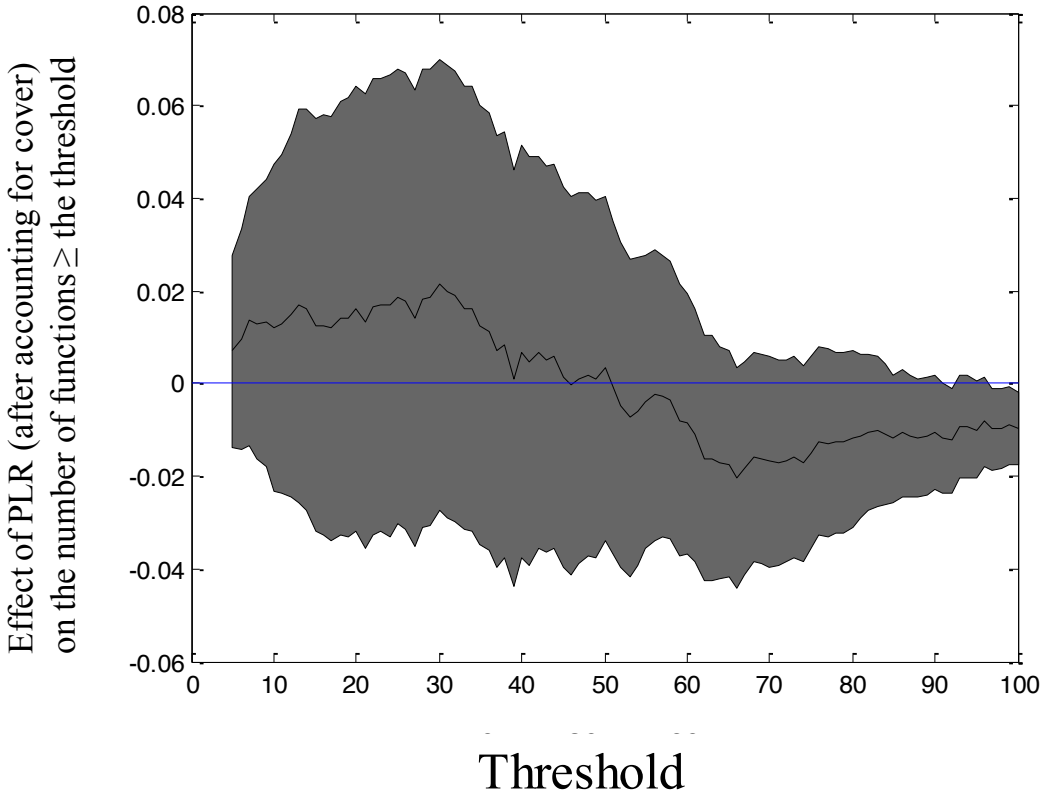

Supplementary Figure 4. **Relationship between patch-size distributions and the number of functions above different thresholds**. Effect of power law relative range (PLR) on the residuals of the number of functions beyond different thresholds after accounting for the effects of total cover (x-axis). The shaded area indicates the 95% confidence intervals of the slope. The blue line indicates the 0 slope line; if this line is within the shaded area no significant effect occurs.

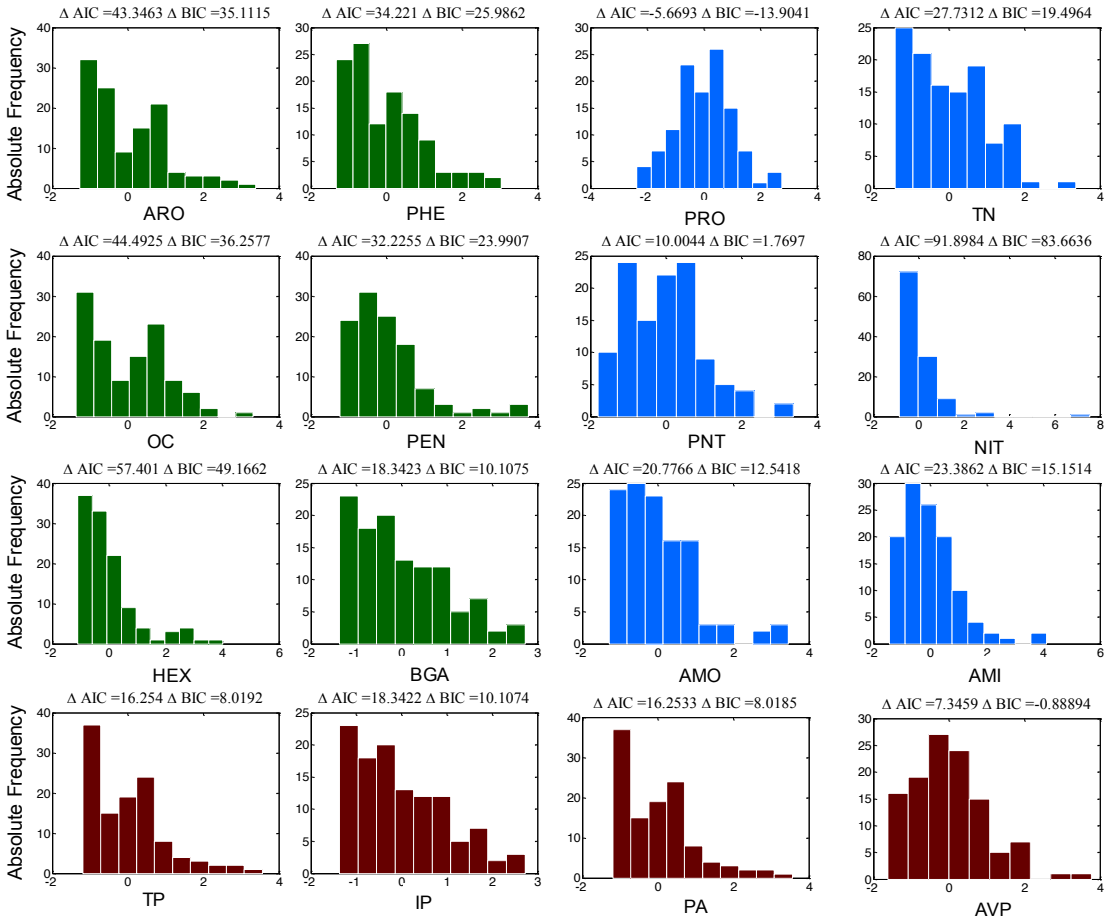

Supplementary Figure 5. Frequency distributions of all functions evaluated. Functions from the carbon, nitrogen and phosphorus cycles are in green, red and blue, respectively. The difference in information criterions (IC; dAIC for Akaike information criterion and dBIC, for Bayesian information criterion) between unimodal and bimodal distributions are shown on top of each panel (in Gaussian mixture models: IC with one mode – IC with two modes; hence positive if bimodal since $IC_2 < IC_1$). PRO: proteins; AMI: amino acids; NIT: nitrates; TN: total nitrogen; OC: organic carbon; TP: total phosphorous; IP: inorganic phosphorous; PA: phosphatase activity; AVP: available phosphorous; BGA: beta-glucosidase activity; ARO: aromatic compounds; PNT: nitrogen transformation rate; PHE: phenols; HEX: hexoses; PEN: pentoses; AMO: ammonium.

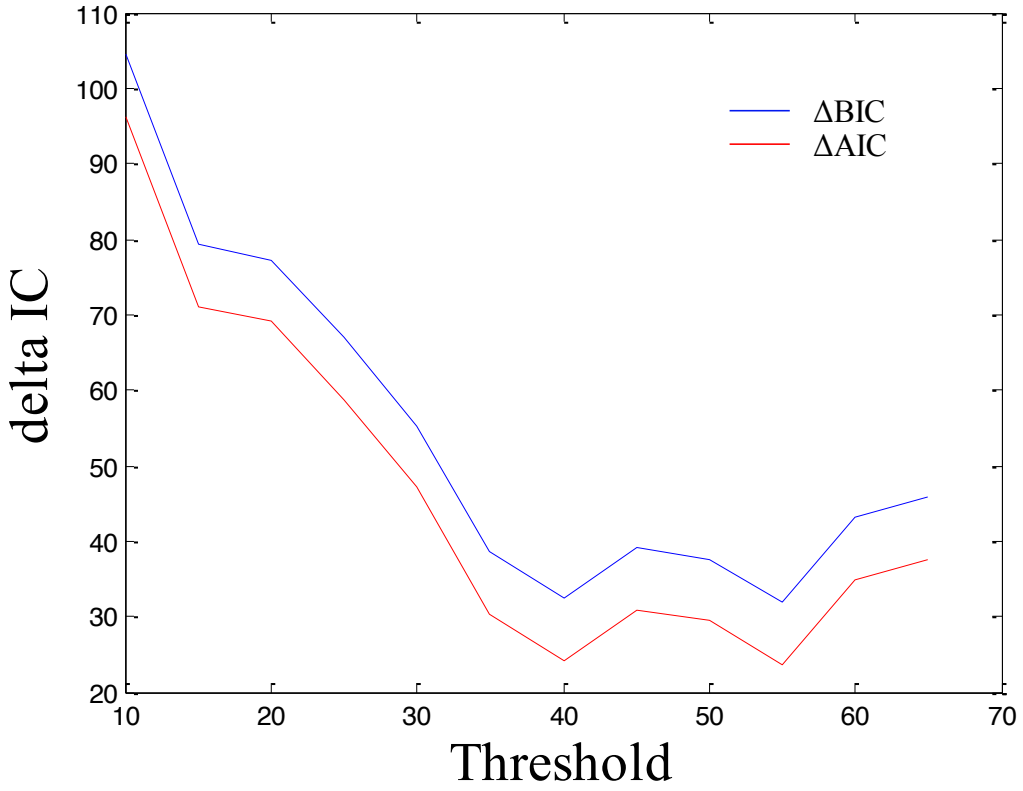

Supplementary Figure 6. **Bimodality in the number of functions above different thresholds**. Differences of information criterions (ΔIC) obtained in a Gaussian mixture models analysis of the number of functions beyond a given threshold respect to their maximum. ΔIC is calculated as IC with one mode – IC with two modes; hence positive if bimodal since $IC_2 < IC_1$.

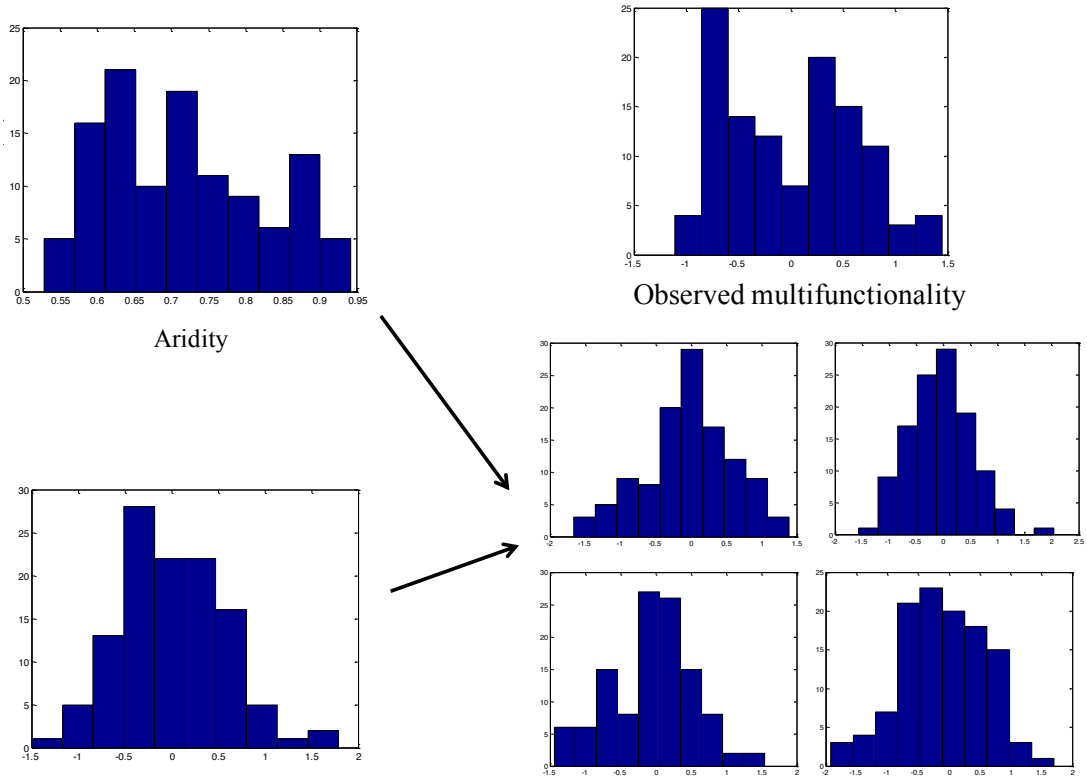

Supplementary Figure 7. Outline of the montecarlo analysis performed to assess effects of the bimodal distribution of aridity on that of multifunctionality. Diagram showing the Monte-Carlo procedure used to generate simulated distributions of multifunctionality (displayed on bottom right) from linear combinations of aridity data (distribution displayed on top left) with the residuals obtained for multifunctionality after controlling for the effect of aridity (distribution displayed in bottom left). The observed distribution of multifunctionality in our 115 study sites is displayed on the top right panel.

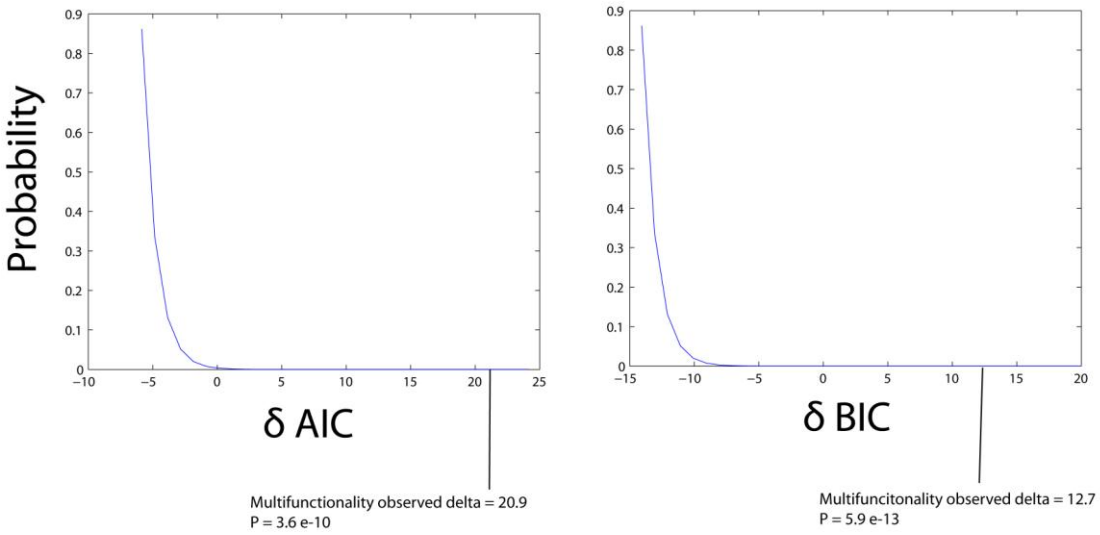

Supplementary Figure 8. **Probability of finding bimodal patterns of multifuncitonality because of aridity**. Probability density functions obtained with the Monte Carlo simulations explained in Supplementary Fig. 7 of different ΔAIC (A) and ΔBIC (B) values. Positive and negative values of ΔAIC and ΔBIC mean bimodal and unimodal distributions, respectively. The values obtained when analyzing the multifunctionality data observed in our study sites are pointed by arrows.

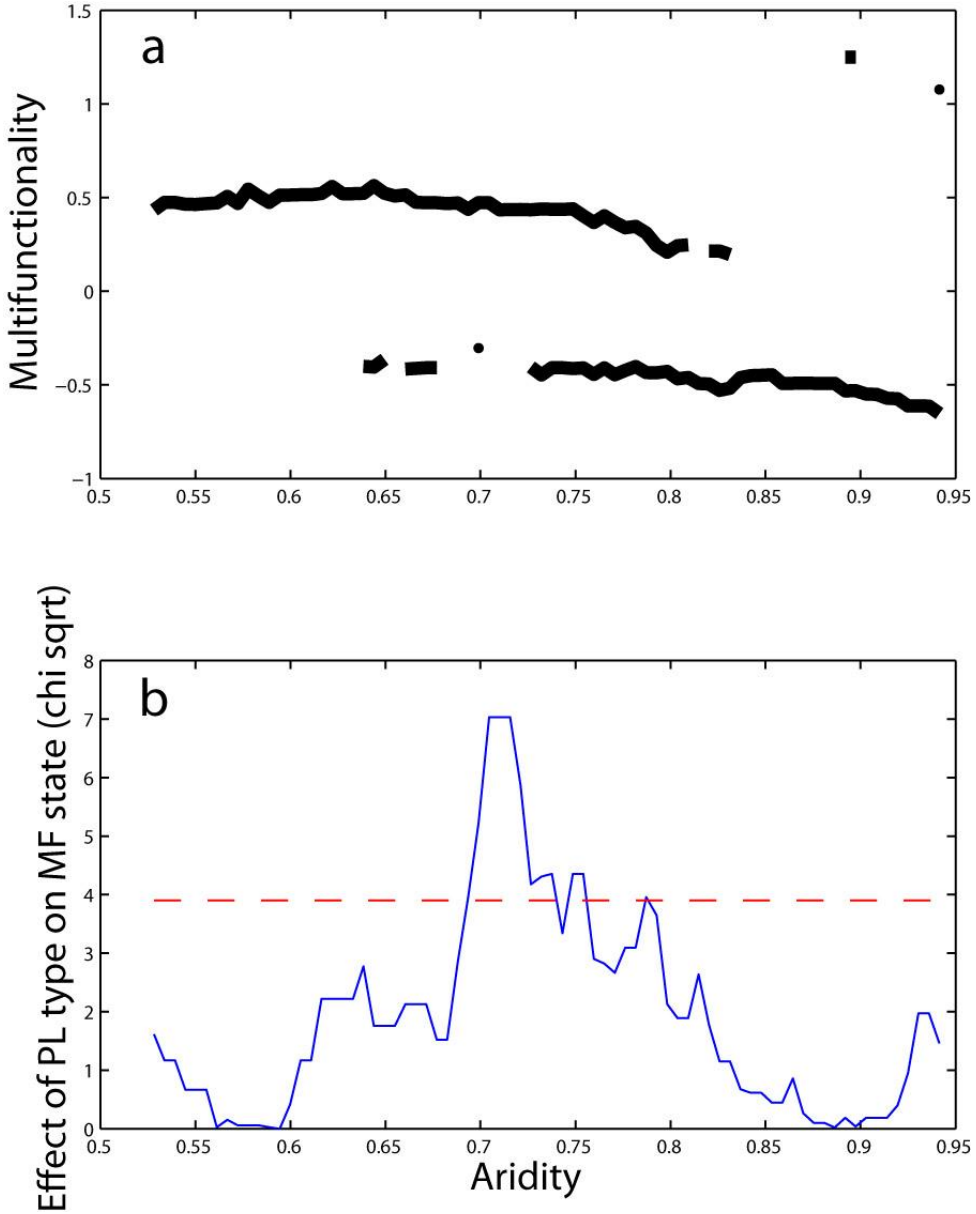

Supplementary Figure 9. **Association between changes in patch-size distributions and multifunctionality across an aridity gradient**. A) Multifunctionality alternative states throughout the aridity gradient studied (computed as local minima of estimated potential energy as in Fig. 4). B) Association between patch size distribution type (PL/non PL-like) and multifunctionality (High /Low) throughout a moving window in aridity. Association is calculated as the Chi-Square metric between both variables. Red dashed line indicate threshold for $P < 0.05$.

Supplementary Tables

Supplementary Table 1. **Linear relationship between patch-size distributions, plant cover and ecosystem functions**. Correlation coefficients of the relationships between different functions and power law relative range (PLR), total cover (TCT) and PLR when accounting by total cover with partial correlations (PLR|TCT). *P* values are shown between brackets and highlighted in bold if below 0.05. PRO: Proteins; AMI: amino acids; NIT: Nitrates; TN: Total Nitrogen; OC: organic carbon; M: multifunctionality; TP: total phosphorous; IP: inorganic phosphorous; PA: phosphatase activity; AVP: available phosphorous; BGA: beta-glucosidase activity; ARO: aromatic compounds; PNT: nitrogen transformation rate; PHE: phenols; HEX: hexoses; PEN: pentoses; AMO: ammonium; M: multifunctionality

			PLR	TCT	PLR|TCT
NITROGEN CYCLE		NIT	-0.03 (0.780)	0.21 **(0.022)**	-0.16 (0.080)
		AMO	0.12 (0.201)	0.39 **(0.001)**	-0.1 (0.267)
		TN	0.3 **(0.001)**	0.48 **(0.001)**	0.07 (0.450)
		PNT	0.2 **(0.031)**	0.33 **(0.001)**	0.04 (0.682)
		AMI	0.11 (0.230)	0.3 **(0.001)**	-0.05 (0.585)
		PRO	0.11 (0.236)	0.24 **(0.011)**	-0.01 (0.877)
CARBON CYCLE		OC	0.34 **(0.001)**	0.54 **(0.001)**	0.08 (0.372)
		PEN	0.29 **(0.001)**	0.28 **(0.002)**	0.18 (0.058)
		HEX	0.13 (0.153)	0.35 **(0.001)**	-0.06 (0.525)
		ARO	0.24 **(0.010)**	0.27 **(0.003)**	0.12 (0.201)
		PHE	0.17 (0.064)	0.31 **(0.001)**	0.02 (0.871)
		BGA	0.23 **(0.014)**	0.38 **(0.001)**	0.04 (0.658)
	PHOSPHOROUS CYCLE	AVP	-0.19 **(0.039)**	-0.08 (0.396)	-0.18 (0.059)
		PA	0.14 (0.125)	0.44 **(0.001)**	-0.11 (0.254)
		IP	0.23 **(0.014)**	0.38 **(0.001)**	0.04 (0.658)
		TP	0.14 (0.125)	0.44 **(0.001)**	-0.11 (0.254)
M			0.26 **(0.006)**	0.53 **(0.001)**	-0.02 (0.8)

109

Supplementary Methods for the manuscript entitled: "Plant spatial patterns identify alternative ecosystem multifunctionality states in global drylands"

Supplementary Methods 1. Image analysis

Although the use of satellite images and aerial photographs has limitations in environments with dense vegetation and when trying to estimate tri-dimensional spatial structures[1], the sparsely distributed plant cover at our study sites allowed us to use Google Earth™ and VirtualEarth™ to achieve the objectives of our study (see also ref. 2,3). Both Google Earth™ and VirtualEarth™ data come from various sources such as satellite images and aerial photos, which present a range of different baseline spatial resolutions, varying from 0.1 m/pixel to 15 m/pixel (e.g., ~0.6 m/pixel of QuickBird imagery, ~0.4 m/pixel of GeoEye imagery, ~0.4-0.5 m/pixel of WorldView imagery, ~0.2 m/pixel of aerial photos, or ~0.3 m/pixel of DigitalGlobe imagery). In our study, we gathered only those images that provided a sufficient resolution to visually identify plant patches (resolution $\leq$ 0.3 m/pixel; with no clouds and homogeneous landscape around; see database in figshare: https://figshare.com/s/3db3640a61ebc975bcda for the resolution of the images used at each site).

We applied the *graythresh* and *im2bw* functions from the image processing toolbox of Matlab to identify an optimum luminance threshold for pixel classification within the image. The *graythresh* function uses Otsu's method for identifying a threshold in the luminance of a gray scale image that minimizes intra-class variance of the black and white pixels[4]. We used this threshold as a first approximation for automatic classification of the image. Then, we classified the image using 30 different thresholds obtained by the k-mean classification analysis[5]. After the automatic classification, we visually checked the images to ensure that the classification was satisfactory. In 17.4%

of the plots, the threshold selected by Otsu's methodology differed in more than 5 k-mean partitions from the one proposed by expert knowledge (which supposed deviations in estimated cover about 5-10%). In such cases we adjusted the luminance threshold to the one proposed by expert knowledge. Lastly, we validated the classifications by comparing the estimated cover of the images with the cover measured in the field. We related field measured cover with that extracted from the first subplot of the images (the one centered in the coordinates of the field survey), and only conserved those of which estimated cover was highly correlated with the one measured in the field (Pearson's $r \approx 0.7$).

Supplementary Methods 2. Trends of variation on patch size distributions

It has been previously documented that patch size distributions fit a power law function (mostly straight line between the logarithm of patch sizes and that of their frequencies[6–8]) and that they depart from these distributions towards truncated power laws when the system is disturbed[7,9]. This means that deviations from power laws should occur only by truncation of the right part of the distribution (i.e., reducing the frequency of big patches in comparison to a pure power law[6,7,9,10]). However, we observed patch-size distributions truncated in both extremes (reduction in the frequency not only of the big, but also of the small, patches). Although not expected in theory, these patch-size distributions truncated at both extremes have been shown in empirical studies[3,11] and in studies simulating low colonization rates of vegetation[12] or high run-off conditions[13]. Our global dataset confirmed these previous results and extended them to a wide variety of dryland communities. Contrary to our expectations, the loss of large patches was coupled with that of small patches (see examples in Supplementary Fig. 1). The loss of small patches with increasing environmental harshness could be explained by

reductions in the number of recruited seedlings under harsh environments[14], or by a low number of isolated individuals in ecosystems dominated by facilitation[15,16]. A low number of patches would reduce statistical power to detect fit to a power law; however, no correlation was found between the number of patches in a site and the parameters of the power law functions fitted ($R^2 = 0.02$, $P = 0.101$).

Supplementary Methods 3. Rationale on the types of patch size distribution

Although the "Power Law Range" (PLR) provided us with a general continuous descriptor of patch size distributions, we wanted to evaluate if there were general types of distributions in our data. Different types of distributions might be reflecting contrasting drivers in vegetation spatial self-organization and, thus, it is worth to explore their functional implications[6,9,17,18]. Because it is not clear what would power law distributions turn into along external disturbances[9,11], nor is possible to compare distributions with different number of samples (which happens because of the existence of x_{min}, although we can compare pure power laws as in Fig. 1b if assuming that this parameter does not exist), we searched for variations in the properties of patch size distributions that could indicate a drastic change in vegetation spatial organization. We found a strong effect of the power law range (PLR) on the rate of decline in the number of patches with their size (α parameter, Fig. 1.a). Power law distributions, however, should be scale invariant, which means that the decay of frequencies with patch sizes (α) should be consistent regardless of the range of patch sizes that fit a power law function[19]. Scale-invariance should be consistent regardless of idiosyncratic differences between study sites (such as the size of the plants, the number of patches or even the total cover of the site[17,20–22]). Therefore, the strong relationship between scale derived metrics (PLR) and α found in our sites was unexpected, and it is likely a consequence of

a change in the processes driving the formation of vegetation spatial patterns. This relationship was driven by a subset of the studied sites with low PLR (Fig. 1.a), which might indicate that these low PLR values are linked to a lack of scale invariance of such distributions. Since this scale invariance (indicated by α values) can only change if the processes forming the spatial distribution are different, we interpreted the discontinuity in the relationship between PLR and α as an indicator of two types of patch size distributions, which differ in the processes driving plant spatial patterns. This rationale is presented in Clauset's et al[19]. Variations in x_{min} will produce variations in α values only if the distribution is not scale-invariant and, therefore, does not fit to a power law.

After splitting the two types of patch size distributions observed, we found two major ranges of PLR, which basically vary in their α values. In one subset PLR and α were not related, as theoretically expected (hereafter we refer to them as power law [PL]-like sites, those with PLR higher than the discontinuity point), and another subset with a strong correlation between PLR and α (hereafter non power law [nonPL]-like sites, those with PLR lower than the discontinuity point, Fig. 1.a). PL-like sites have α values ranging between 2 to 1, similar to other studies fitting power law functions to patch-size distributions of vegetation[6–8,10], and correspond to high PLR values. Hence we have three evidences supporting the classification of PL-like sites as those following a pure power law function: i) scale invariance; ii) α ranges according to previous literature; iii) PLR values closer to 1 (i.e., PL fitting is representative of the overall patch size distribution). Conversely, non PL-like sites have α values > 2, are scale dependent and show poor fits to power law functions (i.e., low PLR distributions, showing typically more curved like distributions). When compared with the relative fitting of pure power law (power law fitting without x_{min}) across the full PLR range (see

Fig. 1.b), the threshold found in PLR vs α with our methodology (0.57) was very similar to that found for the sign shift of the fitted line of the former regression.

Because our conclusions depend on the threshold found for patch size distribution types, we performed a sensitivity analyses to: i) examine the consistency of this threshold to different methodologies; and ii) test whether slight variation of this threshold affected our main result (chi squared test of multifunctionality types versus patch size distribution types). Both methods fit discontinuous regressions with a breaking point that changes its slope (known also as piecewise regressions), following equation S1.

$$\alpha = intcp_1 - \beta_1 * PLR \; iff \; PLR \geq PLR_{thres}$$

$$\alpha = intcp_2 - \beta_2 * PLR \; iff \; PLR < PLR_{thres} \qquad \text{equation S1}$$

Where two linear regressions containing intercept (intcp) and slopes (β) as parameters relate α and PLR depending on a breaking point (PLR_{thres}) from which the slopes are significantly different.

First, we used the iterative model selection procedure of Crawley [23], which looks at different break points in a discontinuous model (equation S1) and minimizes the residual mean squared errors. Second, we used the package "segmented" in R [24], which is specifically designed to look at piecewise regression for breaking points. Both approaches yielded similar breaking points values (PLR = 0.58 and 0.62± 0.06, respectively) to the value originally found (PLR = 0.57). This variation in breakpoints makes some of the sites to shift from PL-like to nonPL-like (two if considering Crawley approach, ten if considering segmented package approach).

To test if these different thresholds could affect our main results and conclusions, we performed a chi-squared test between multifunctionality states and patch size distribution types with these two new breakpoints, and still found significant

associations for both the breakpoint using Crawley's approach (χ^2 = 7.79 , p = 0.005) and the breakpoint using segmented package (χ^2 = 8.94, p = 0.003). This shows that our results are robust to the methodology used to detect thresholds in the fit of patch size distributions to a power law.

Additional support for the division of patch size distribution types conducted is provided by the SEM analysis we performed after this classification and is discussed in the main manuscript (Fig. 2).

Supplementary Methods 4. Additional information on the meaning of the potential function

Stability in a physical system is often represented by the potential energy function of such system. This function represents the energy of a state variable, and, in a dynamical system, we may interpret it as the "odds to change" of that variable[25]. Local minima in potential functions represent dynamically "stable" states of the variable, whereas the other values will tend towards a stable state according to the shape of the potential (moving always from high potential values to lower values[25]).

We consider that there is a generic underlying stochastic system driven dynamically, such that a potential function is yielded in the form:

$$dz = -U(z)dt + \sigma dW \qquad \textbf{equation S2}$$

where z corresponds to the state variable (multifunctionality), U is the potential function representing the dynamical energy of the system as a function of its own state, σ is the noise level and dW is a noise term emerging from a Wiener process. The Fokker-Planck equation connects the probability density to the potential of the underlying model, so that the potential might be derived as[26]:

$$U' = -\frac{\sigma^2}{2}\log\left(PDF\right) \qquad \textbf{equation S3}$$

Supplementary Methods 5. Sensitivity analysis of bimodality in multifunctionality

To test the robustness of the alternative states in multifunctionality found, we performed three additional sensitivity analyses. With them we aimed to test whether the bimodal pattern of multifunctionality was: (i) maintained regardless of the approach used for measuring multifunctionality, (ii) not a consequence of the subset of sites for which we could find good quality images and (iii) not confounded by the distribution of a key driver of multifunctionality such as aridity.

Multifunctionality can be measured either by analyzing separate functions independently, with the averaging approach described above, or by evaluating the number of functions that reach single[27] or multiple[28] thresholds. We assessed the robustness of our findings to all these different approaches available to estimate multifunctionality. First, we performed Gaussian mixture models on all the functions separately (normalized as Z-scores to ease interpretation of the results, Supplementary Fig. 5). Second, we transformed the Z-scores of each function to percentage from the maximum (5% percentile of maximum values for each function to avoid outliers), and obtained the number of functions beyond a given threshold. We used thresholds from 5 to 100%, and obtained the distributions of the number of functions beyond these thresholds. Then we applied Gaussian mixture models to find the number of modes in the number of functions above the threshold (Supplementary Fig. 6). The histograms of the number of functions above thresholds higher than 65% produced too few bins to perform a reliable Gaussian mixture analysis (almost all sites only had 0-3 functions higher than 65% respect to the maximum values), so this analysis was performed using thresholds from 5 to 65%. We assessed the bimodality by subtracting the BIC for unimodality and bimodality in a Gaussian mixture approach using Matlab. This metric,

called ΔBIC, is positive if bimodality is achieved, and negative if the resulting simulated distribution is unimodal.

The results of these analyses confirmed that bimodality is consistent regardless of the method employed for assessing multifunctionality. They also show that bimodality is probably caused by several of the functions we measured (phenols, aromatic compounds and organic carbon, phosphatase activity, total nitrogen and total phosphorous). By using the threshold approach[28] we found that bimodality in ecosystem multifunctionality remains when measuring it as the number of functions exceeding multiple thresholds instead of the averaging index.

We also evaluated whether the two alternative states in multifunctionality found were caused by the particular subset of sites selected for this study. For doing so, we further analyzed multifunctionality values obtained for the entire dataset from Maestre et al.[29]. Multifunctionality was also bimodal when using the 224 sites of this dataset instead of the 115 used here (BIC for one and two modes were 366.7 and 365.2 respectively; and AIC 359.8 and 348).

Although bimodality might be interpreted as the existence of two different alternative states, it may also be confounded by a bimodal distribution of the drivers of multifunctionality. This is unlikely, as the two multifunctionality states co-occurred across a range of aridity values (see Fig. 4 in the manuscript). Nevertheless we conducted sensitivity analyses, based on Monte-Carlo randomizations, to control for this potential confounding factor. We performed a regression between multifunctionality and aridity, obtained the parameters describing this relationship and a distribution of the residuals from this regression. By using these parameters and the aridity data, and by adding random residuals generated from the residuals distribution obtained, we simulated 1000 theoretic sets of multifunctionality values derived from a

linear combination of aridity (Supplementary Fig. 7). We assessed the bimodality of these generated values by using the ΔBIC metric (positive if bimodality is achieved). Our results show that most of the simulations were unimodal, meaning that the bimodality in ecosystem multifunctionality we found in our analyses is highly unlikely ($P = 3.6 \cdot 10^{-10}$) to have been driven by a confounding effect of the bimodal distribution of aridity in our data (Supplementary Fig. 8). The same simulations using AIC instead of BIC yielded very similar results ($P = 5.9 \cdot 10^{-13}$).

Supplementary Methods 6. Analyzing the relationships between ecosystem functions

To better understand the mechanisms driving the two alternative states in ecosystem multifunctionality found, we assessed the relationship between each individual function within the two multifunctionality states, as well as the relationships between functions and multifunctionality state (Fig. 3.b). We expected tighter relationships between functions in the high multifunctionality state, as soil functions in high functional systems usually covariate strongly with each other[30]. We also expected a differential role of functions associated to each major nutrient cycle (C, N and P) as drivers of ecosystem multifunctionality due to the changes in nutrient stoichiometry of soils observed in disturbed or arid systems[30,31]. This occurs because different soil nutrients usually relate to similar metabolic pathways (e.g., N and C are biotically driven whereas P is mostly driven by abiotic processes[32,33]). A switch in the control of a specific soil function over the others can be induced by changing the limiting factors in these soil processes[34] or by delimiting biogeochemical cycles to episodic water inputs[35]. In particular, phosphorus and nitrogen/carbon nutrient pools may uncouple under arid conditions, exhibiting a shift in the dominating factors from carbon/nitrogen in low

aridity (biotically controlled) sites to phosphorus in high aridity (abiotically controlled) sites[30].

Supplementary Methods 7. Controlling for the potential confounding effect of aridity on the association between types of patch-size distribution and multifunctionality

Both patch-size distribution types and multifunctionality states are influenced by aridity. As such, the association between these variables could be confounded by their common response to aridity. To evaluate the association between patch size distribution and multifunctionality types along the different levels of aridity studied, we performed the Chi-square tests described in the main text (association between High/low multifunctionality and PL-like /nonPL-like types of patch size distributions), but across a moving window through aridity. To do so, we first ordered the sites from low to high aridity values; we then took a subset of the 40 less arid sites and performed the Chi-square test. This step was repeated iteratively by sequentially discarding the first site (less arid) and adding the next more arid site through all our study sites. We found that the association between patch size distribution and multifunctionality types peaked around aridity values of 0.7 (Supplementary Fig. 9). These aridity values corresponded to those around which in the two multifunctionality states co-occurred. Moreover, since these ranges of aridity (0.65-0.8) are the ones in which aridity related more poorly to multifunctionality, we can exclude any confounding effect from aridity on the relationship between patch size distribution and multifunctionality.

References

1. Lefsky, M. A., Cohen, W. B., Parker, G. G. & Harding, D. J. Lidar Remote Sensing for Ecosystem Studies Lidar, an emerging remote sensing technology that directly measures the three-dimensional distribution of plant canopies, can accurately estimate vegetation structural attributes and should be of particular inter. *Bioscience* **52,** 19–30 (2002).
2. Xu, C. *et al.* Can we infer plant facilitation from remote sensing? A test across global drylands. *Ecol. Appl.* **25,** 1456–1462 (2015).
3. Quets, J. J. *et al.* Unraveling landscapes with phytogenic mounds (nebkhas): An exploration of spatial pattern. *Acta Oecologica* **49,** 53–63 (2013).
4. Otsu, N. Thresholds selection method form grey-level histograms. *IEEE Trans. Syst. Man Cybern.* **9,** 62–66 (1979).
5. Solomon, C. & Breckon, T. *Fundamentals of Digital Image Processing: A practical approach with examples in Matlab*. (John Wiley & Sons, 2011).
6. Scanlon, T. M., Caylor, K. K., Levin, S. A. & Rodriguez-Iturbe, I. Positive feedbacks promote power-law clustering of Kalahari vegetation. *Nature* **449,** 209–212 (2007).
7. Lin, Y., Han, G., Zhao, M. & Chang, S. X. Spatial vegetation patterns as early signs of desertification: a case study of a desert steppe in Inner Mongolia, China. *Landsc. Ecol.* **25,** 1519–1527 (2010).
8. Moreno de las Heras, M., Saco, P. M., Willgoose, G. R. & Tongway, D. J. Assessing landscape structure and pattern fragmentation in semiarid ecosystems using patch-size distributions. *Ecol. Appl.* **21,** 2793–2805 (2011).
9. Kéfi, S. *et al.* Spatial vegetation patterns and imminent desertification in Mediterranean arid ecosystems. *Nature* **449,** 213–217 (2007).
10. Kéfi, S. *et al.* Robust scaling in ecosystems and the meltdown of patch size distributions before extinction. *Ecol. Lett.* **14,** 29–35 (2011).
11. Bowker, M. A., Maestre, F. T. & Mau, R. L. Diversity and patch-size distributions of biological soil crusts regulate dryland ecosystem multifunctionality. *Ecosystems* **16,** 923–933 (2013).
12. Marani, M. *et al.* Spatial organization and ecohydrological interactions in oxygen-limited vegetation ecosystems. *Water Resour. Res.* **42.** DOI: 10.1029/2005WR004582 (2006).
13. von Hardenberg, J., Kletter, A. Y., Yizhaq, H., Nathan, J. & Meron, E. Periodic versus scale-free patterns in dryland vegetation. *Proc. R. Soc. London B Biol. Sci.* **282.** DOI: 10.1098/rspb.2009.2208 (2010).
14. Weltzin, J. F. & McPherson, G. R. Facilitation of conspecific seedling recruitment and shifts in temperate savanna ecotones. *Ecol. Monogr.* **69,** 513–534 (1999).
15. Bertness, M. D. & Callaway, R. Positive interactions in communities. *Trends Ecol. Evol.* **9,** 191–193 (1994).
16. Soliveres, S. *et al.* Functional traits determine plant co-occurrence more than environment or evolutionary relatedness in global drylands. *Perspect. plant Ecol.*

399 *Evol. Syst.* **16,** 164–173 (2014).

400 17. Manor, A. & Shnerb, N. M. Facilitation, competition, and vegetation patchiness:
401 from scale free distribution to patterns. *J. Theor. Biol.* **253,** 838–842 (2008).

402 18. Bowker, M. A. & Maestre, F. T. Inferring local competition intensity from patch
403 size distributions: a test using biological soil crusts. *Oikos* **121,** 1914–1922
404 (2012).

405 19. Clauset, A., Shalizi, C. R. & Newman, M. E. J. Power-law distributions in
406 empirical data. *SIAM Rev.* **51,** 661–703 (2009).

407 20. Brown, J. H. *et al.* The fractal nature of nature: power laws, ecological
408 complexity and biodiversity. *Philos. Trans. R. Soc. London B Biol. Sci.* **357,** 619–
409 626 (2002).

410 21. Gisiger, T. Scale invariance in biology: coincidence or footprint of a universal
411 mechanism? *Biol. Rev. Camb. Philos. Soc.* **76,** 161–209 (2001).

412 22. Rietkerk, M., Dekker, S. C., de Ruiter, P. C. & van de Koppel, J. Self-organized
413 patchiness and catastrophic shifts in ecosystems. *Science (80-.).* **305,** 1926–1929
414 (2004).

415 23. Crawley, M. J. *The R book*. (John Wiley & Sons, 2012).

416 24. Muggeo, V. M. R. segmented: an R Package to Fit Regression Models with
417 Broken-Line Relationships. *R News* **8,** 20–25 (2008).

418 25. Strogatz, S. H. *Nonlinear dynamics and chaos: with applications to physics,*
419 *biology, chemistry, and engineering*. (Westview press, 2014).

420 26. Livina, V. N. & Lenton, T. M. A modified method for detecting incipient
421 bifurcations in a dynamical system. *Geophys. Res. Lett.* **34.** DOI:
422 10.1029/2006GL028672 (2007).

423 27. Zavaleta, E. S., Pasari, J. R., Hulvey, K. B. & Tilman, G. D. Sustaining multiple
424 ecosystem functions in grassland communities requires higher biodiversity. *Proc.*
425 *Natl. Acad. Sci.* **107,** 1443–1446 (2010).

426 28. Byrnes, J. E. K. *et al.* Investigating the relationship between biodiversity and
427 ecosystem multifunctionality: challenges and solutions. *Methods Ecol. Evol.* **5,**
428 111–124 (2014).

429 29. Maestre, F. T. *et al.* Plant species richness and ecosystem multifunctionality in
430 global drylands. *Science (80-.).* **335,** 214–218 (2012).

431 30. Delgado-Baquerizo, M. *et al.* Decoupling of soil nutrient cycles as a function of
432 aridity in global drylands. *Nature* **502,** 672–676 (2013).

433 31. Wang, C. *et al.* Aridity threshold in controlling ecosystem nitrogen cycling in
434 arid and semi-arid grasslands. *Nat. Commun.* **5.** DOI: 10.1038/ncomms5799
435 (2014).

436 32. McGill, W. B. & Cole, C. V. Comparative aspects of cycling of organic C, N, S
437 and P through soil organic matter. *Geoderma* **26,** 267–286 (1981).

438 33. Finzi, A. C. *et al.* Responses and feedbacks of coupled biogeochemical cycles to
439 climate change: examples from terrestrial ecosystems. *Front. Ecol. Environ.* **9,**
440 61–67 (2011).

441 34. Vitousek, P. M., Porder, S., Houlton, B. Z. & Chadwick, O. A. Terrestrial
442 phosphorus limitation: mechanisms, implications, and nitrogen-phosphorus

interactions. *Ecol. Appl.* **20,** 5–15 (2010).

35. Austin, A. T. *et al.* Water pulses and biogeochemical cycles in arid and semiarid ecosystems. *Oecologia* **141,** 221–235 (2004).